On tungsten redeposition at the divertor target

A.V.Chankin, D.P.Coster, and R.Dux

Max-Planck-Institut für Pasmaphysik, Boltzmannstraße 2, 85748 Garching bei München, Germany

Abstract

Recent modeling of controlled ELMs in ITER with tungsten (W) divertor target plates by SOLPS code package predicted high electron temperatures (> 100 eV) and densities (> $1\times10^{21}m^{-3}$) at the outer target. Under certain scenarios W sputtered during ELMs can penetrate into the core in quantities large enough to cause deterioration of the discharge performance, as was shown by coupled SOLPS5.0/STRAHL/ASTRA runs. The *net* sputtering yield, however, was expected to be dramatically reduced by the 'prompt redeposition' during the first Larmor gyration of W^{+1} *(Fussmann et al., 1995)*. Under high n_e/T_e conditions at the target during ITER ELMs prompt redeposition would reduce W sputtering by factor $p^{-2} \sim 10^4$ (with $p \equiv \tau_{ion}\omega_{gyro} \sim 0.01$). This relation however doesn't include effects of multiple ionizations of sputtered W atoms and electric field in the magnetic pre-sheath (MPS, or 'Chodura sheath') and Debye sheath (DS). Monte-Carlo simulations of W redeposition with the inclusion of these effects are described in the paper. It is shown that for $p << 1$ inclusion of multiple W ionizations and electric field in the MPS and DS changes physics of W redeposition: from geometrical effects of circular gyro-orbits hitting the target surface to mainly energy considerations: potential barrier for ions escaping into the main plasma. The overwhelming majority of ions are being drawn back to the target by a strong attracting electric field. It is also shown that a possibility of W self-sputtering avalanche can be ruled out due to smallness of sputtered W energies compared to incident energies (as neutrals/ions circulate in the MPS) which doesn't compensate for the kinetic energy gain of ions in the MPS/DS, leading to a sharp reduction in sputtering yields. Results of simulations are applicable to a wide range of plasma conditions at the target plates that can be encountered in various magnetic confinement fusion devices.

1. Introduction

Tungsten is presently the material of choice for the divertor of the International Thermonuclear Experimental Reactor (ITER) (see [1] and refs. therein). In the preparation for the installation of W divertor target plates, the place in the divertor subject to most severe particle and heat loads, ITER is coordinating research on various aspects of W behaviour in the divertor. Of a particular concern is sputtering of the W target plate surface under high transient plasma particle and heat exposures during Edge Localised Modes (ELMs) and its subsequent penetration into the plasma core, where it can extinguish the fusion reaction due to its high radiation heat losses (see [2] and refs. therein). These issues were addressed in recent simulations of W behaviour under various ITER operational scenarios carried out with the suite of predictive codes: SOLPS, STRAHL and ASTRA, to be reported later. Physical sputtering of the W target during controlled ELMs was modeled by the 2D multi-fluid edge transport code SOLPS (SOLPS5.0/B2 version was used) [3]. The simulations were carried out first under the assumption that all sputtered W enters the divertor plasma and is

transported into the main scrape-off layer (SOL), and then by taking into account prompt redeposition of the W ions in their first Larmor orbit. The inclusion of W prompt redeposition in the SOLPS modeling is observed to have a dramatic effect on the W content in the plasma, providing for at least a factor 10^4 reduction in the amount of W arriving in the pedestal from an ELM event. Prompt redeposition has a particularly large effect in ITER ELMs because of the high plasma density (> 1×10^{21}m^{-3}) and high electron temperature (> 100 eV) near the divertor targets resulting in a short ionization mean free path for the sputtered neutral W.

After prompt W redeposition is taken into account, the remaining W flux into the plasma can be calculated as the product of the initially sputtered W flux and the fraction of non-redeposited W, often referred to as 'non-redeposition' and equal to 1 minus the fraction of redeposited W. One way to calculate non-redeposition (the non-redeposition fraction $f_{non-redep}$) is to use a formula originally proposed by *Fussman et al.* [4]. This formula assumes ideally flat target surface, only one ionization (1st ionization of an atom with no subsequent ionizations), constant n_e/T_e above the target, cosine distribution of sputtered atoms, magnetic field (B-field) parallel to the surface, and ignores electric field (E-field) in the plasma. Its derivation is based entirely on geometrical effects: the probability of a circular ion gyro-orbit launched at different distances above the surface and at different angles to hit the target surface. The original formula [4] after algebraic transformations can be expressed in a more compact form [5] which will be used below:

$$f_{non-redep} = \frac{p^2}{1+p^2}\ , \tag{1}$$

where

$$p = \tau_{ion}\omega_{gyro} = \lambda_{ion} / \rho_{W^+,max}. \tag{2}$$

Here τ_{ion} is ionization time of neutral tungsten (W^0), ω_{gyro} is the angular gyro-frequency of the W^{+1} ion, λ_{ion} is the ionization length of W^0, and $\rho_{W^+,max}$ is the W^{+1} Larmor radius calculated for the case when ion velocity is perpendicular to the B-field.

For small *p*, which is the case with ITER ELMs, where $p \sim 10^{-2}$, non-redeposition scales with p^2, being numerically ~ 10^{-4}. However, already in [4] it was pointed out that for $p << 1$ there is a high probability of multiple ionizations, so that the particles can get ionized several times before terminating the first orbit, leading to a reduction in prompt redeposition. Ref. [4] also summarized experience with Monte Carlo calculations with the ERO code [6] where multiple ionizations and E-field in the magnetic pre-sheath (MPS) and Debye sheath (DS) were included. The presence of the E-field tends to *increase* redeposition by attracting ions to the target, but the associated density drop (when one assumes Boltzmann distribution of density in the electric potential) tends to *reduce* redeposition. As was concluded it [4], the two latter effects largely compensate each other and the dependence of redeposition on *p* turns out to be quite similar to that obtained from Eq. (1). These simulations however were aimed at reproducing experimental conditions of ASDEX Upgrade, without taking into account ELMs, and a rather modest $p = 0.45$ was assumed.

Hyodo et al. [7] carried out Monte Carlo simulations of prompt W redeposition including multiple ionizations for a wide range of *p*, but without taking into account electric field. For $p \to 0$, contrary to predictions of Eq. (1), the redeposition fraction in these simulations didn't approach unity (non-redeposition didn't approach zero), instead approaching ≈ 0.4. As will be shown later, however, for small *p* inclusion of electric field in the MPS (to a larger extent) and DS (to a lesser extent) has a dramatic effect on the redeposition/non-redeposition fraction, so simulations without taking them into account are almost irrelevant.

Recent 1D kinetic modeling of the JET SOL with tungsten divertor plates by *Tskhakaya et al*. [8] confirmed importance of the E-field near the surface in the reduction of the net W erosion, which represented only ~ 1% of the gross W erosion. It was also shown that those W ions that escape the prompt redeposition do not propagate far away into the plasma from divertor plates and are returned back to them by the friction force with the main ions.

In this work, the emphasis is made on W redeposition in a very close proximity to the target, at distances not exceeding the MPS width, without attempting to trace W motion in the main SOL and divertor plasma. The results should provide non-redeposition fractions ($f_{non-redep}$ coefficients) that could be used by SOLPS and similar edge codes to determine net W fluxes into the plasma. Here by 'plasma' one understands all divertor, scrape-off layer (SOL) and inner core regions of the plasma (inside the magnetic separatrix or limiter) that are covered by the numerical grid. This 'plasma' ends at the entrance to the MPS, where boundary conditions are imposed. Electric field and friction forces exerted on W ions beyond the MPS entrance, counting from the target surface, are supposed to be properly described by the edge codes.

In this paper, the model for W redeposition simulations is described in section 2, results of simulations with zero electric field are described in section 3, simulations with the inclusion of the E-field as a part of the MPS model are described in section 4, results for the newly introduced 'total redeposition' (as opposed to 'prompt redeposition') are described in section 5, simulations for the two different MPS models are compared in section 6, and the possibility of W self-sputtering avalanche is discussed in section 7. Finally, conclusions are drawn in the Summary section (Sec. 8).

2. Tungsten redeposition model

As is common with tungsten redeposition studies, we assume an ideally flat target surface and oblique angles between the B-field and the surface. Sputtered neutral tungsten atoms (W^0) are emitted/launched in all directions from the launch position on the surface. Kinetic energy of W^0 is fixed. The launch direction is characterized by angles φ and θ in spherical coordinate system, as shown in figure 1. At some distance away from the launch position W^0 is ionized. This position is determined in the rectangular (Xs,Ys,Zs) coordinate system with Xs and Ys axes lying within the target surface ('s' stands for 'surface'), with Zs axis coinciding with the projection of the B-field onto the target surface. The distance between the place of the ionization and the launch point (origin of the (Xs,Ys,Zs) coordinate system), normalized to $\rho_{W^+,max}$, coincides with the *p* parameter Eq. (2). For cases without electric field and uniform density distribution the ionization distance will be assumed fixed ($= p \times \rho_{W^+,max}$). For cases *with* electric field and variable density the ionization position is

calculated at each time step by using the probability of ionization $\Delta t / \tau_{ion}$, with Δt being the time step.

A fine mesh in φ, θ angles with Δφ = Δθ = 1° was used. The 'cosine' distribution of sputtered W was assumed (given by sin(φ)×sin(θ)), and solid angles ~ Δ(cos(θ)) in the spherical coordinate system were taken into account to ascribe statistical weights to runs. 25 runs were done for each launch direction, with the total of $25 \times 180^2 = 8.1 \times 10^5$ orbits calculated for each choice of electron temperature T_e and *p* parameter. Ionization coefficients for W^0 and each subsequent ionization state (W^{+z}) were taken from [9]. A wide range of T_e's and *p*'s was covered in the simulations, with T_e values = 3, 10, 30, 100, 300 and 1000 eV, and *p* values = 0.01, 0.03, 0.1, 0.3, 1, 3, 10.

After the first ionization, W ion motion is followed in the rectangular (X,Y,Z) coordinate system aligned with B-field: Z axis is parallel to the B-field, see figure 2. A coordinate transformation between the (Xs,Ys,Zs) and (X,Y,Z) systems is performed by rotating about the Xs,X common axis by angle α– the angle between the B-field and the target surface. The system of equations for the ion orbit following is:

$$\begin{cases} \Delta V_x = \dfrac{Z_i e B}{m_W c} V_y \Delta t \\ \Delta V_y = -\dfrac{Z_i e B}{m_W c} V_x \Delta t + \dfrac{Z_i e E_y}{m_W} \Delta t \\ \Delta V_z = \dfrac{Z_i e E_z}{m_W} \Delta t \\ \Delta x = V_x \Delta t, \quad \Delta y = V_y \Delta t, \quad \Delta z = V_z \Delta t \end{cases} \tag{3}$$

This simple system of equations accounts for Lorenz and electric field forces. Electric field is assumed perpendicular to the surface, so E_x=0 (x-direction is along the target surface). Elementary charge *e* is assumed to be positive. Small time step $\Delta t = 10^{-4} / \omega_{gyro}$ was used in all calculations ensuring good kinetic energy conservation.

3. Simulations with zero electric field and uniform density (no MPS)

During W ion orbit calculations, at each time step there is a finite probability of the next ionization: $Z_i \rightarrow Z_i+1$, calculated for a given plasma n_e and T_e. A random number generator is used to increase the ion charge. An example of a W ion orbit launched perpendicular to the B-field, which in turn is parallel to the surface, and with an angle 45° with respect to the normal to the surface ($\theta = 135°$) is shown in figure 3. The orbit starts at a distance $p = 0.01 \times \rho_{W^+,max}$ from the origin (x = y = 0, with the z-coordinate being irrelevant). T_e = 22.6 eV was used. Calculations were interrupted some time after the W ion acquired the charge state +7. This figure demonstrates why redeposition is expected to be smaller when multiple ionizations are taken into account: each subsequent ionization reduces the size of the orbit, with high Z_i orbits located some distance away from the surface, thereby reducing the probability of the orbit's intersection with the surface. Without multiple ionizations, the orbit launched with parameters as shown in Fig. 3 would be absorbed by the surface. In the

simulations described in this paper orbits were only followed until they either crossed the surface or the local minimum of the y-position was reached while the ion was still above the surface. Correspondingly, the result was counted either towards redeposited or non-redeposited orbits, with weighting factors accounting for the cosine distribution of sputtered atomic W and solid angles in the (φ,θ) space. For a special test case where multiple ionizations were prohibited and only W^{+1} motion allowed, non-redeposition fractions were found to be in a good agreement with Eq. (1).

Table 1 shows results of orbit calculations for a number of p and T_e values for the case with the B-field parallel to the target: $\alpha = 0°$. The top number in each cell gives the non-redeposition fraction $f_{non-redep}$: the fraction of orbits (with the inclusion of aforementioned weighting factors) that were not promptly redeposited. For small p the numbers deviate strongly from Eq. (1). For p = 0.01, T_e = 100 eV, which will be referred to below as ITER ELM parameters, the non-redeposition fraction is ≈ 0.38. The number in the middle of each cell gives the average charge of promptly redeposited W ions at the time when they hit the target surface, and the bottom number – the average W charge for non-redeposited ions at the first local minimum of their distance from the surface (local minimum in the y-direction), when calculations were interrupted. As one can see, for ITER ELM parameters average Z_i is around 5 – 7.

Results shown in Table 1 should replace Eq. (1), since they represent the natural extension of this formula onto the case with multiple W ionization, and were obtained under the same other assumptions, including the assumption of a constant distance between the point of the first ionization and the launching position at the target surface, which in these calculations is given by $p \times \rho_{W^+,max}$. These results however are largely irrelevant since they don't take into account the E-field in the MPS and DS which makes a profound impact on the non-redeposition fraction for small p values, as will be shown in the next section. For this reason it is not worth expanding on these results, for example by repeating calculations for angles between the B-field and the target surface different from 0°.

4. Simulations with inclusion of electric field and density variation in the magnetic pre-sheath (MPS)

We are only interested in cases with oblique angles α between the B-field and the target surface, relevant to ITER equilibria and divertor design aimed at minimizing particle and heat loads on the divertor target plate. Results of kinetic modeling of the MPS were reviewed in the book by P.C.Stangeby [10] (p.98). As the angle between the B-field and the surface is reduced the electric potential drop is more and more concentrated in the MPS rather than the Debye sheath (DS). Moreover, in his recent study of the MPS [11] Stangeby shows that for angles α = 1 - 5° the DS almost disappears and electric potential drop occurs almost entirely in the MPS. This should have a beneficial effect of increasing the redeposition fraction for small p since it becomes less probable that a sputtered W neutral would get ionized outside of the region of strong electric fields near the target.

The normalized value of density in the MPS as a function of the distance from the target normalized to ion Larmor radius is shown in figure 4, replicated from [11]. The ion mass equal to 2 amu and $T_e = T_i$ are assumed. For the Larmor radius, $\rho_i = c_s / \omega_i$ was used, with

$c_s = \sqrt{(T_e + \gamma T_i)/m_i}$ and γ = 1, hence $\rho_i = \sqrt{2T_i/m_i}/\omega_i$. In addition to the results of the Stangeby's MPS model, the "Brooks' model" curve corresponding to the model [12] is plotted. In the SOLPS modeling of ITER ELMs [3] the main ion species were deuterium, with some fraction of tritium and a smaller fraction of hydrogen. The angle between the B-field and surface was ≈ 3° at both, inner and outer divertor targets. We will be assuming in the simulations deuterium plasma and $\alpha = 3°$. Hence, one of the curves of the Stangeby's model shown in Fig. 4 can be the basis of the MPS model used here.

Figure 5 shows normalized density from the Stangeby's MPS model for $\alpha = 3°$ (Fig. 5) and its interpolation used in the present study. Both curves are plotted versus the normalized distance from the surface. The interpolation curve corresponds to the MPS width of exactly $10\rho_i$ (for D^+ ions), at which distance n/n_o = 1. For the electric potential profile, Boltzmann distribution will be assumed.

The total potential drop across the MPS and DS doesn't depend on α and is given by [10,11]:

$$\frac{e\Delta\Psi}{kT_e} = 0.51 \times \ln\left[2\pi\left(\frac{m_e}{m_i}\right)\left(1+\frac{T_i}{T_e}\right)\right]. \qquad (4)$$

For T_e = T_i and m_i = 2 amu, $e\Delta\Psi = 2.84 \times kT_e$. The interpolation curve shown in Fig. 5 corresponds to $e\Delta\Psi = 2.80 \times kT_e$. Hence, almost all the potential drop occurs in the MPS.

Unlike the situation in cases without electric field and with uniform density distribution, considered in the previous section, where velocity of sputtered W atoms didn't influence the redeposition probability, simulations with the E-field in the MPS require introduction of a new parameter: the ratio of sputtered W^0 energy to some energy characterizing the potential distribution in the MPS and DS. Here we introduce the ratio of the W^0 energy to the averaged ion energy at the entrance to the MPS, $3/2kT_i$:

$$R_E = \frac{\xi_{W^0}}{3/2kT_i}. \qquad (5)$$

In the simulations described below, reduction of the plasma density in the MPS is included in the ionization probability. Parameter *p* refers to its value at the MPS entrance where plasma density reaches its maximum. The energy ratio $R_E = 0.3$ and the angle between the B-field and the surface $\alpha = 3°$ will be assumed if not otherwise stated. The $R_E = 0.3$ assumption probably exaggerates this ratio, as follows from the data on energies of sputtered W presented in Sec. 7. Friction forces between W ions and D^+ will not be taken into account. This is justified by the fact that these forces compete with the E-field force outside of the MPS, while the E-field is dramatically increased and becomes the dominant player in the narrow layer of the MPS. With all assumptions adopted and numerical scheme used, calculations below represent full Monte Carlo simulations, with the exceptions of the fixed W sputtered energy and pre-determined launch angles (φ,θ) selection. These however are rather advantages of the simulations: W^0 energy can be varied by varying the energy ratio R_E, and convolution of results obtained for different R_E can be performed later. While the set of

launch angles (φ,θ) with adopted statistical weights represents a theoretical limit in eliminating statistical noise that can be achieved with an infinite number of launched orbits.

Table 2 shows W non-redeposition fractions (top numbers in each cell) for the case with multiple ionizations and an E-field from the Stangeby's MPS model for $\alpha = 3°$ and $R_E = 0.3$. The meaning of middle and bottom numbers in each cell is the same as in Table 1. Since for $p = 0.01$ all orbits intersected the target, the bottom numbers for this column don't apply and NaN values were generated. The introduction of the E-field in the MPS clearly leads to a dramatic reduction of the non-redeposition fraction for cases with small p. For $p = 0.03$, small non-redeposition numbers of order 10^{-5} are very imprecise due to a limited number of orbits not intersecting the target, resulting in large statistical errors.

The main reason why non-redeposition fractions at small p in Table 1 are so low is an extremely large E-field in the part of the MPS adjacent to the target ($\sim \rho_i$). To understand how multiple W ionizations together with the E-field in the MPS increase the probability of prompt redeposition, it is useful to plot a few individual orbits. Figure 6 shows examples of three orbits: the (largest, black) orbit calculated without E-field and multiple ionizations, the (medium sized, red) orbit calculated without the E-field but with multiple ionizations, with the final charge $Z_i = 7$, and the (smallest, blue) orbit calculated with both the E-field in the MPS and multiple ionizations, with the final charge $Z_i = 3$. The smallest orbit doesn't show features of the Larmor rotation, as an ion doesn't rotate clockwise, being attracted to the target by the strong E-field right after the first ionization of the neutral W. Its relatively small final charge, $Z_i = 3$, compared to $Z_i = 7$ for the medium sized orbit is due to both the density drop near the target which reduced the probability of ionizations, and its small path. Superimposed onto the orbits are horizontal dashed lines indicating deuterium Larmor radius and the end of the MPS which coincided with $10\rho_i$. The smallest orbit lies fully inside the first deuterium Larmor radius distance from the target. After the first ionization, an ion could only move by a distance $< 1/3\rho_i$ away from the surface where it has lost all its kinetic energy perpendicular to the surface. The E-field has essentially imposed a potential barrier on the upward motion of the ion. The strongest E-field is found inside of the first ρ_i: the normalized density n/n_o increases from 0.06 (at the target) to 0.28 inside this layer, which translates into the potential difference (owing to $e\Psi = kT_e \ln(n/n_o)$) of $\Delta\Psi \approx 1.5 \times kT_e/e$. Such a strong E-field removed all ion kinetic energy in the direction normal to the surface in $< 1/3\rho_i$ (keep in mind that the total initial kinetic energy on an ion was $R_E \times 3/2kT_e \approx 1/2kT_e$ in these calculations).

5. 'Prompt redeposition' and 'total redeposition'.

'Prompt redeposition', defined as an ion's return to the target during its first gyro-motion, doesn't properly describe the action of the MPS in returning ions to the target. At angles $\alpha > 0°$ electric field inside the MPS has a parallel component attracting an ion to the target. An ion may have not been redeposited after the first gyro-motion, but if its kinetic energy is insufficient to leave the MPS it will be redeposited after a few more gyrations as it will be moving towards the target along the B-field. Since perpendicular (to the B-field) energy on an ion is constant it these simulations, only the ion's parallel kinetic energy in the direction away from the target matters here. Namely, if

$$\xi_{\|,W^{+Z_i}} + Z_i e\Psi < 0\,, \qquad (6)$$

then an ion will not overcome the potential barrier in the MPS and will be returned to the target. In the present simulations, for ions that were not promptly redeposited calculations of their sum of parallel kinetic and potential energies was done during the first gyro-motion, at the local low of an orbit (in the y-direction; and this was the point at which orbit calculations were interrupted for the middle sized orbit shown in Fig. 6). And if at this point the condition Eq. (6) was fulfilled, such a promptly non-redeposited ion was counted towards 'total redeposition', which is a new term introduced here. In reality, some ions which according to the condition Eq. (6) were capable of leaving the MPS, while moving along the B-field away from the target will be ionized again, resulting in the increase of the potential barrier and their ultimate return to the target. Such situations however were not considered in the present simulations, and ions' motion was always interrupted at local lows of their orbits. Therefore, the 'total redeposition' calculated here provides only an upper limit for the non-redeposition fraction, and such simulations can be considered as providing a 'conservative estimate' for the non-redeposition, in the sense that the real non-redeposition may be smaller, while the redeposition - larger.

The total non-redeposition fractions calculated for the same conditions as were assumed in the previous section, with results shown in Table 2, are shown in Table 3 (top numbers). As one can see, for small p the total non-redeposition is significantly smaller than the prompt non-redeposition. Unlike in tables 1 and 2, only two numbers are shown in each cell of Table 3, with the bottom number giving the ratio of the average kinetic energy of ions hitting the target divided by the kinetic energy of sputtered W^0. These ratios may be interpreted as 'energy amplification factors' reflecting a kinetic energy gain acquired by ions that were first sputtered as W^0 at (lower) energies, but after multiple ionizations gained (higher) energies in the electric potential before returning to the target. The effect of the energy amplification for W ions circulating in the MPS might potentially cause a self-sputtering avalanche discussed in Sec. 7.

6. Brooks' vs. Stangeby's MPS model

In this section simulations are repeated for the Brooks' MPS model in order to assess which MPS model predicts larger redeposition. Such a comparison also provides a sensitivity study to assess how strongly results depend on the choice of a particular MPS model.

In the Brooks' MPS model, normalized density drops only to ≈ 0.12 at the target, implying a potential difference across the MPS $\Delta\Psi = -kT_e/e \times \ln\left[(n/n_o)\big|_{target}\right] \approx 2.12 \times kT_e/e$. This is less than $\Delta\Psi = 2.84 \times kT_e/e$ - the potential difference across both MPS and Debye sheath (DS) calculated according to Eq. (4). The Brooks' model therefore assumes a potential drop $\Delta\Psi \approx 0.72 \times kT_e/e$ across the DS. In order to decide whether the presence of the DS can make an impact on the redeposition, one has to estimate its width. For T_e=100 eV, n_e= $5\times10^{20}\,m^{-3}$, parameters of ITER ELMs that would correspond to p = 0.01 for B = 5.3 T (ITER magnetic field on axis), the ratio of the Debye length (∝ DS width) to the W^+ Larmor radius (∝ MPS width) is $\lambda_D/\rho_{W^+} \approx 10^{-3}$. The DS therefore appears to be too narrow to make a significant impact on the W redeposition: its width is by more than an order of magnitude

smaller than the ionization length of a neutral W, which in turn is longer than $p \times \rho_{W^+,max} \approx 10^{-3} \times \rho_{W^+,max}$ owing to density reduction near the target surface which reduces the ionization probability. If however the DS under certain conditions turns out to be important for redeposition calculations, its influence will be to *increase* the redeposition, and its neglect will therefore provide a conservative estimate for the non-redeposition fraction, meaning that the real non-redeposition can even be smaller than in our simulations.

The fact that n/n_o at the target in the Brooks' MPS model is larger than in the Stangeby's model should contribute towards larger redeposition in the Brooks' model owing to shorter ionization lengths of the sputtered neutral W. On the other hand, the E-field near the target is larger in the Stanbeby's model (despite the n/n_o profile is less steep in this model, n/n_o value at the target is lower and this leads to a larger E-field), which should contribute towards larger redeposition in this model for low p. Simulation results show that both prompt and total redepositions are larger in the Stangeby's MPS model for all T_e and p values, implying that the most important factor for increasing redeposition is large E-field near the target. In this section we present only results for the total redeposition. Total non-redeposition fractions (top numbers) and energy amplification factors (see previous section) are shown in Table 3 for the Brooks' MPS model. They are obtained for the same parameters as those used in results shown in Table 2: $\alpha = 3°$, $R_E = 0.3$. Linear interpolation for the n/n_o profile tabulated from Fig. 4 was implemented in the simulations.

The Debye sheath was not completely ignored in the simulations with the Brooks' MPS model. Due to a significant potential drop in the DS, kinetic energy gain $Z_i e \Delta\Psi_{DS}$ was included in the calculations of kinetic energy with which ions hit the target, with Z_i taken at the end of the orbit calculations.

In the rest of this paper, instead of doing simulations for both MPS models, a choice will be made in favour of the Brooks' model for the only reason that it predicts smaller redeposition than the Stangeby's model. With non-redeposition fractions being already very small, not only for ITER ELM parameters but even for substantially larger p values, we thereby again adopt a conservative approach by making choices that can reduce predicted redeposition fractions. Also, simulations will only be done for the 'total redeposition' as a more relevant parameter than the 'prompt redeposition'. We would like to note, however, that physics-wise it is the more recent Stangeby's MPS model that should be given preference over the Brooks' model. The latter, for example, assumes a constant ratio of electrical potential drops across the MPS and DS, independent of the α angle, whereas the former (correctly) describes larger share of the potential drop across the MPS for smaller α angles. Similar simulations using Stangeby's MPS model were also performed in this study, but the results are not included in the paper.

Table 4 gives the same results as in Table 3 but for the Brooks' MPS model. There are substantial differences in absolute numbers for total non-redeposition fractions between results of the two models for small p values: 0.3 and especially 0.1, but they don's change the results qualitatively: non-redeposition is extremely low for small p in both models and have similar dependencies on p and T_e.

In addition to comparing the results of the two MPS models, sensitivity studies were also done by varying angle α between 0 and 6° within the same MPS model (with the same sharing between potential drops across MPS and DS). The results were almost insensitive to

the α variation. Finally, for each MPS model simulations were performed with the width of the MPS reduced by factor $\sqrt{2}$ (which was done due to an initial erroneous assumption that $\rho_i = \sqrt{T_i / m_i}$ was implied as the D^+ ion Larmor radius in Fig. 4 (ref. [11]) instead of $\rho_i = \sqrt{2T_i / m_i}$). For the narrower MPS width non-redeposition fractions were found to be somewhat larger, but the differences in the non-redeposition fractions introduced by the MPS width variation were much smaller than the differences between the two MPS models.

The magnitude of the sputtered neutral W kinetic energy is expected to have a significant effect on the non-redeposition fraction. In the simulations presented here, W^0 kinetic energy was varied by varying parameter R_E given by Eq. (5). Figure 7 shows total non-redeposition fractions versus p for T_e = 100 eV, for four values of R_E. Absence of data points at p = 0.01 and 0.03 for R_E = 0.1 and 0.3 implies zero non-redeposition obtained in the simulations. Similarly, the sputtered W^0 energy has a large impact on the 'energy amplification factor' (see Sec. 5), which is the factor of increase of kinetic energy of originally sputtered W^0 after its ionization in the MPS and subsequent acceleration in the MPS and DS. Energy amplification factors are shown in Fig. 8 for T_e = 100 eV, for four values of R_E. In Figs. 7 and 8, simulations were done by using Brooks' MPS model.

7. Possibility of W self-sputtering avalanche

Dependence of the sputtering yield for W self-sputtering on the projectile/impact (ion or neutral) energy for normal incidence is shown in figure 9, calculated according to the revised Bohdansky formula [13]. For high impact energies, above 1 keV, sputtering yield becomes > 1. High Z_i tungsten ions approaching the divertor target from the main SOL may acquire high impact energies due to acceleration in the MPS and DS. For example, for Z_i = 10 and T_e = 100 eV an ion will acquire energy of $\approx Z_i \times 3 \times T_e$ = 3 keV, enough to sputter more than one W neutral from the target. W ions can also acquire high impact energies by the friction drag force exerted on them by the main ion flow towards the target with the ion sound speed c_s. The acquired W ion energy can be a fraction of $m_W c_s^2 / 2$, which for $c_s = \sqrt{(T_e + T_i)/m_i}$ and $T_e = T_i$ is equal to $T_i m_W / m_i$, or $92 \times T_i$ for a deuterium plasma. In addition, other impurity atoms can also cause W sputtering. Therefore, for sufficiently high T_e/n_e near the target surface there is bound to be a certain amount of W sputtered from the W surface. The most potentially dangerous process for both target sputtering and contamination of the core plasma is the W self-sputtering avalanche by W circulating in the MPS. In this process the originally sputtered W^0 would get ionized within the MPS and acquire large enough energy in the electric field to sputter more than one W^0 from the surface, thereby triggering a self-sputtering avalanche.

Self-sputtering avalanche can be triggered when the yield for W self-sputtering starts to exceed unity. In order to assess the probability of this happening, one needs to compare two factors: the factor of a decrease of W energy caused by sputtering (ratio of the sputtered W^0 energy to the impact W ion energy) and the factor of an increase of W energy caused by acceleration in the MPS and DS (ratio of the impact W ion energy due to its acceleration in the MPS and DS to the sputtered W^0 energy, an 'energy amplification factor', see Sec. 5). It is the product of these two factors that will determine whether W energy will increase of decrease during its circulation in the MPS. An increase would invariably lead to a self-

sputtering runaway process, after W kinetic energy exceeds the threshold at which the self-sputtering yield = 1.

We assume that particles sputtered from the surface have Thomson energy distribution [14]. Figure 10 shows mean (a) and maximum (b) energy of sputtered W^0 as a function of projectile (impact) energy for various bombarding species, including W itself (thick curves marked with "m_p = 184"), for normal incidence, based on the model [14]. The most relevant for this study is Fig. 10a for the mean energy of sputtered W versus projectile W energy. For 5 keV impact W energy, the mean sputtered W energy is ≈ 35 eV, which represents < 1% of the projectile energy. For 1 keV impact energy, the sputtered energy is ≈ 18 eV, representing < 2% of the projectile energy. The maximum in the ratio of the sputtered to projectile W energy, 2.6%, is reched at the projectile energy of ≈ 300 eV, but the sputtering yield for such projectile energies is already substantially below 1 (see Fig. 9). Overall, we may conclude that the factor of decrease in W energy caused by sputtering is ~ 100.

The factor of an increase of W energy caused by acceleration in the MPS and DS can be obtained from Fig. 8 which shows 'energy amplification factors' introduced in Sec. 5. For small *p*, factors of an energy increase are ~ 10. With the product of the two ratios determining the probability of the W self-sputtering avalanche ~ 10×1/100 = 1/10, one should expect a quick reduction of the energy for W circulating in the MPS. So, even if the initial impact W energy is large enough to sputter a few W atoms, an avalanche leading to an exponential growth of sputtered W can be ruled out, for all *p* at T_e = 100 eV. The same conclusion can be drawn from analyzing energy amplification factors for other T_e's in the entire range of 3 – 1000 eV (not included in this paper).

Finally, we provide the most conservative evaluation of the W self-sputtering possibility by analyzing maximum energies of sputtered W (shown in Fig. 10b), keeping in mind that it is an absolute minority of W atoms emitted from the surface that has such high energies. Let's for example consider the case of $T_e = T_i$ = 200 eV, Z_i = 10. The W^{+10} ion acquires kinetic energy $Z_i \times 3 \times T_e$ = 6 keV before hitting the target. Let's assume that it is sputtered from the target surface with the maximum possible energy. From the dependence of the maximum energy on the projectile energy (Fig. 10b) one can estimate the maximum sputtered W^0 energy to be 6000×0.14 = 840 eV. After an ionization in the MPS and acceleration in the E-field the W ion is expected to acquire a kinetic energy according to the 'energy amplification factor' which depends on the R_E parameter (Eq. 5) calculated as 840/300 = 2.8. This R_E parameter is close to R_E = 3 for which the results are shown in Fig. 8, with energy amplification factors not exceeding 3. Hence, the ion will hit the target again with the kinetic energy ≈ 840×3 = 2520 eV, which is by factor ≈ 2.4 lower than the impact kinetic energy of the original W^{+10} ion. These estimates show that even under most pessimistic, even unrealistic, assumptions, aimed at increasing the energy of W in the process of its circulation in the MPS, W energy is still being reduced by > factor 2 in one cycle.

8. Summary

Under high n_e/T_e conditions near the divertor target, with $p = \tau_{ion}\omega_{gyro} << 1$, inclusion of multiple W ionizations and an electric field force in the magnetic pre-sheath (MPS) changes physics of the W redeposition: from geometrical effects of circles intersecting the surface to mainly energy barrier considerations. Typically, sputtered W atoms have relatively low

energies, and an electric potential barrier imposed by the electric field in the MPS prevents W ions from entering the main plasma, beyond the entrance to the MPS. For ITER target conditions predicted by SOLPS modeling of controlled ELMs, with T_e ~ 100 eV and p ~ 0.01, W redeposition is close to 100%. In addition to the prompt redeposition, results were also obtained for the 'total redeposition' accounting for the fact that even for ions that can complete the first gyro-orbit without hitting the surface there is a large probability of them being attracted to the surface by parallel electric field after a few more gyrations. The results of the simulations show that also for less dense/hot conditions at the target, with p ~ 0.1, the 'total non-redeposition' is rather low, typically not exceeding 0.01 or even less, depending on the MPS model used, and provided the kinetic energy of sputtered W atoms is only a fraction of the T_i at the entrance to the MPS, the condition fulfilled for the overwhelming majority of sputtered W^0.

Under ITER ELM conditions, a significant W target sputtering can be caused by high Z_i ions of various impurities (including W itself) entering the MPS from the main SOL plasma, for which the sputtering yield can exceed unity. At the same time, analysis based on energies of W ions striking the target, energies of W^0 sputtered from the target, and calculations of energy amplification factors which account for a kinetic energy gain in the MPS/DS of W ions compared to the sputtered W^0 energy, indicates a significant safety margin against a possibility of W self-sputtering avalanche, the process in which circulation of W in the MPS/DS would lead to progressively higher W energies above those for which W self-sputtering yield = 1.

References

[1] R.A.Pitts, S.Carpentier, F.Escourbiac, et al., "A full tungsten divertor for ITER: physics issues and design status", Proc. 20th PSI Conference, Jülich, 2012, paper I4 (to appear in J. Nucl. Mater.), http://dx.doi.org/10.1016/j.jnucmat.2013.01.008.

[2] A.Loarte, G.Huijsmans, S.Futatani, et al., "Progress on the application of ELM control schemes to ITER scenarios from the non-active phase to DT operation", report ITR/1-2 presented at the 24th IAEA Fusion Energy Conference, 8-13 October 2012, San Diego, USA

[3] D.P.Coster, A.V.Chankin, H.-J.Klingshirn, X.Bonnin, A.Kukushkin, A.Loarte, "SOLPS modeling of controlled ELMs for ITER", submitted to 40th European Physical Society Conference on Plasma Physics, Helsinki, Finland, July 1st-5th 2013.

[4] G.Fussman, W.Engelhardt, D.Naujoks, et al., in: Proceedings of the 15th International Conference of Plasma Physics and Controlled Nuclear Fusion Research, IAEA, Viena, vol. 2, 1995, p. 143.

[5] R.Dux, A.Janzer, T.Pütterich, Nucl. Fus. **51** (2011) 053002.

[6] D.Naujoks, J.Roth, K.Krieger, G.Lieder, M.Laux, J. Nucl. Mater. **210** (1994) 43.

[7] I.Hyodo, M.Hirano, K.Miyamoto, K.Hoshino, A.Hatayama, J. Nucl. Mater. **313–316** (2003) 1183–1187.

[8] D.Tskhakaya, M.Groth, and JET EFDA contributors, '1D kinetic modeling of the JET SOL with tungsten divertor plates', Proc. 20th PSI Conference, Jülich, 2012, to appear in J. Nucl. Mater. (2013), http://dx.doi.org/10.1016/j.jnucmat.2013.01.108.

[9] S.D.Loch, J.A.Ludlow, M.S.Pindzola, A.D.Whiteford and D.C.Griffin, Phys. Rev. A, **72** (2005) 052716.

[10] P.C.Stangeby, in *The Boundary of Magnetic Fusion Devices*, IOP Publishing, Bristol (2000).

[11] P.C.Stangeby, Nucl. Fus. **52** (2012) 083012.

[12] J.N.Brooks, Phys. Fluid B **2** (1990) 1858.

[13] W.Eckstein, C.García-Rosales and J.Roth, Nucl. Instrum. Methods Phys. Res. B **83** (1993) 95.

[14] M.W.Thomson, Phil. Mag. **18** (1968) 377.

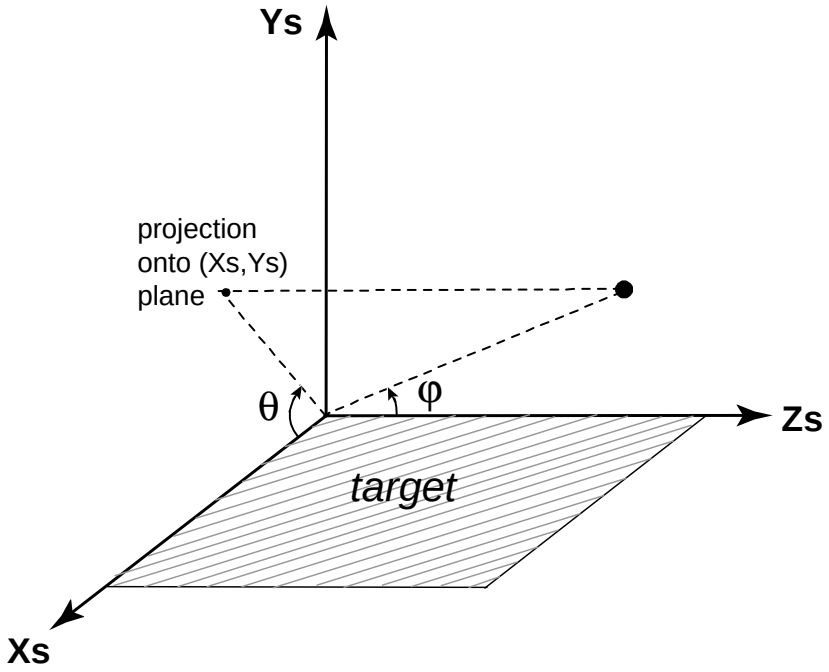

Figure 1. Coordinate systems used for launching W atoms from the surface (see text for details). Axis Zs coincides with the projection of the B-field onto the target surface.

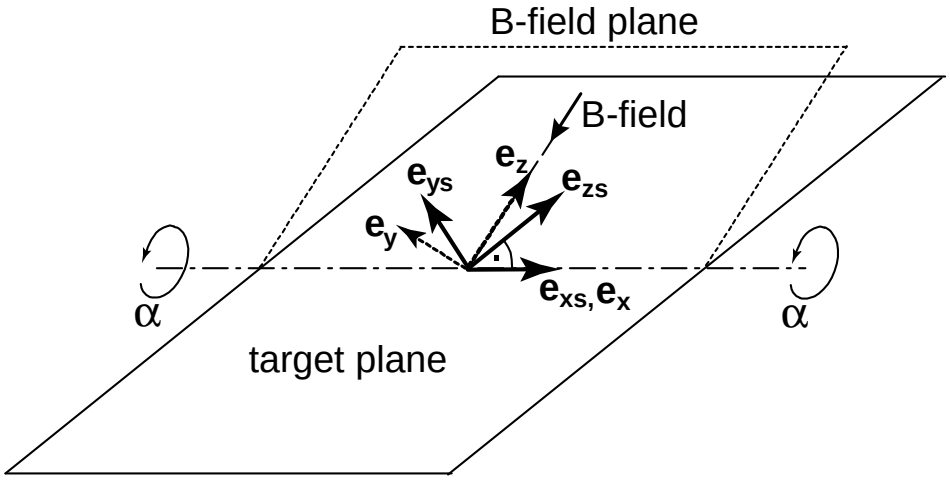

Figure 2. Transformation of the coordinate system (Xs,Ys,Zs) with $\boldsymbol{e}_{xs}$,$\boldsymbol{e}_{zs}$ lying in the target plane, into the coordinate system (X,Y,Z), with $\boldsymbol{e}_{xs}$,$\boldsymbol{e}_{zs}$ lying in the B-field plane, with $\boldsymbol{e}_z$ parallel to the B-field. The transformation is made by rotating the target plane by angle α (angle between the B-field and the target surface) about the common Xs,X axis.

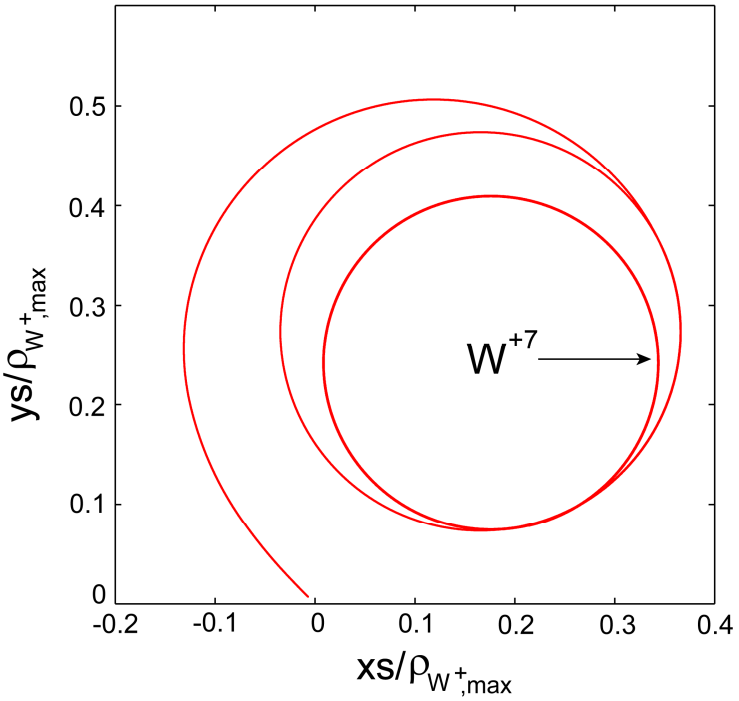

Figure 3. Example of an orbit launched with p=0.01, φ=90°, θ=135°, B-field parallel to the surface (α=0°), in the plasma with T_e=22.6 eV. Calculations were interrupted at W charge state +7.

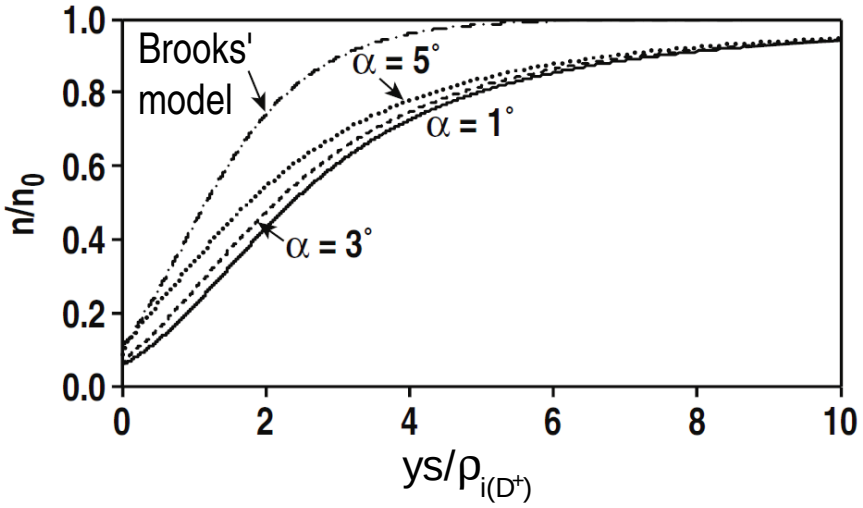

Figure 4. The normalized value of density in the MPS as a function of the distance from the target normalized to ion Larmor radius. Ion mass equal to 2 amu is assumed. α is the angle between the B-field and the surface. The "Brooks's model" curve corresponds to the model [12]. The figure is replicated from ref. [11] with some alterations in the notations.

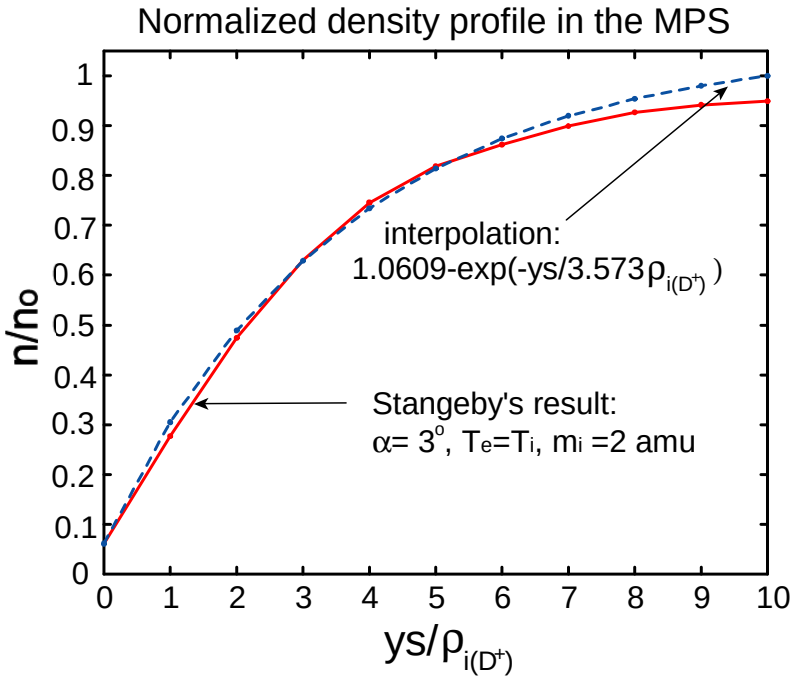

Figure 5. The normalized value of density in the MPS for Stangeby's model (see Fig. 4) with $\alpha = 3°$ and its interpolation used in the simulations described in this paper, vs. the normalized distance from the target surface.

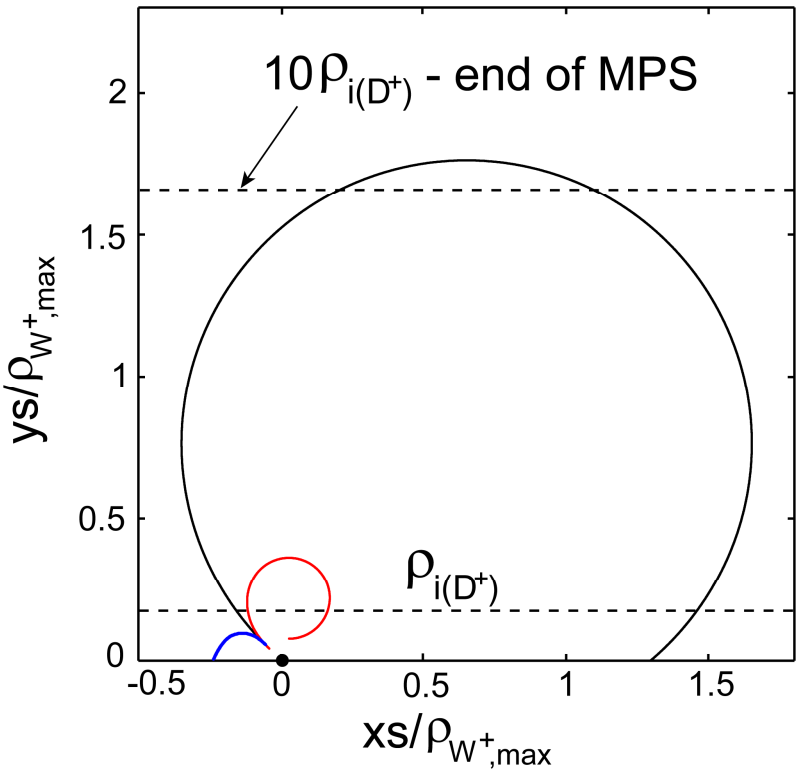

Figure 6. Examples of individual orbits for p = 0.01, T_e = 100 eV, R_E = 0.3, φ=90°, θ=135°, and B-field parallel to the surface (α=0°). Largest orbit (black, redeposited) – for the case with no E-field, no multiple ionizations, medium orbit (red, non-redeposited) – for the case with no E-field, but with multiple ionizations, smallest orbit (blue, redeposited) – for the case with both E-field and multiple ionizations.

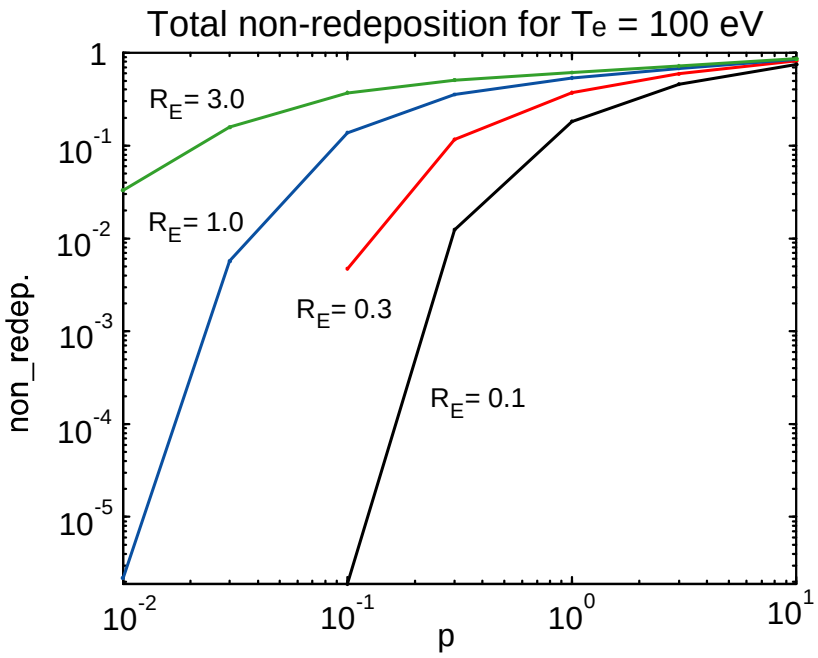

Figure 7. Total non-redeposition fractions vs. p for T_e = 100 eV, for four values of R_E. Angle between the B-field and the target surface α=3°. Brooks' MPS model is used. Absence of data points at p = 0.01 and 0.03 for R_E = 0.1 and 0.3 implies zero non-redeposition obtained in the simulations.

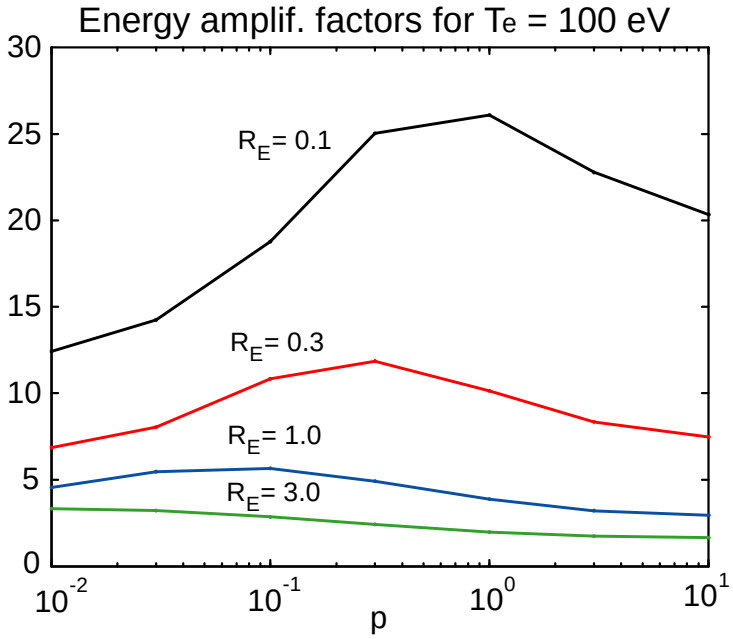

Figure 8. Energy amplification factors vs. p for T_e = 100 eV, for four values of R_E. Angle between the B-field and the target surface α=3°. Brooks' MPS model is used.

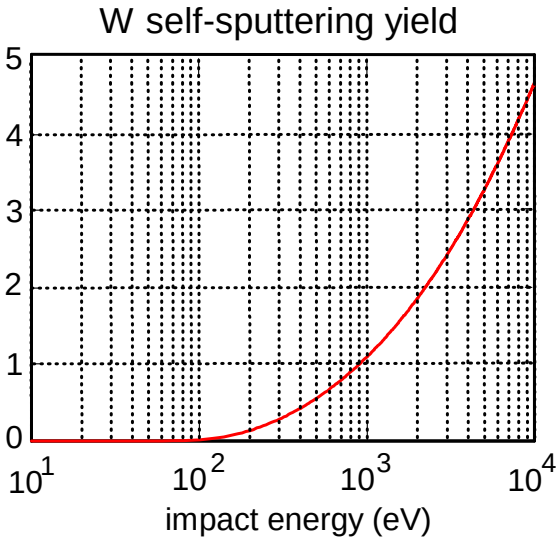

Figure 9. Dependence of sputtering yield for W self-sputtering on the impact projectile energy.

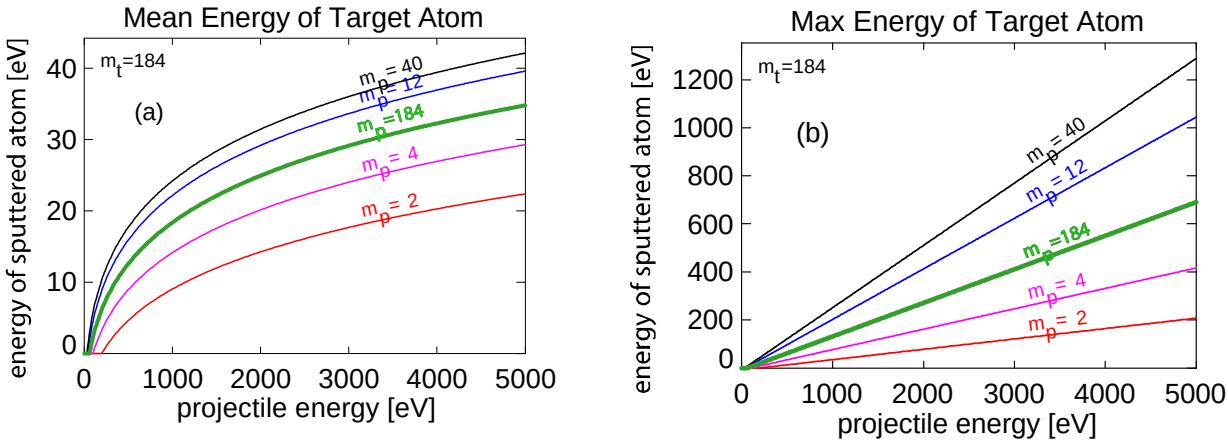

Figure 10. Mean (a) and maximum (b) energy of sputtered W^0 as functions of the projectile/impact energy for various bombarding species, including W itself (thick curves marked with "m_p = 184").

p→ Te (eV)↓	0.01	0.03	0.1	0.3	1	3	10
3	**0.1569** 2.0405 2.3270	**0.2970** 1.8948 2.0696	**0.3099** 1.4511 2.0111	**0.2457** 1.1370 1.8309	**0.5313** 1.0293 1.2084	**0.9011** 1.0086 1.0532	**0.9909** 1.0026 1.0155
10	**0.3194** 3.6063 4.1113	**0.3721** 2.9327 3.5946	**0.4176** 2.2613 2.9012	**0.5255** 1.7442 2.3003	**0.6516** 1.1885 1.7859	**0.9095** 1.0506 1.2914	**0.9910** 1.0152 1.0916
30	**0.3198** 4.7546 5.5699	**0.4255** 3.9931 4.6430	**0.5347** 3.0118 3.8532	**0.6117** 2.1486 2.9736	**0.7260** 1.3559 2.1451	**0.9169** 1.0919 1.4918	**0.9912** 1.0286 1.1634
100	**0.3838** 5.7183 6.7161	**0.4588** 4.5509 5.5344	**0.5677** 3.3880 4.3123	**0.6495** 2.3682 3.3114	**0.7577** 1.4524 2.3347	**0.9209** 1.1203 1.6021	**0.9913** 1.0354 1.2043
300	**0.4278** 6.2019 7.8142	**0.4686** 4.7506 5.9309	**0.5724** 3.5188 4.4751	**0.6620** 2.4665 3.4284	**0.7716** 1.5079 2.4125	**0.9228** 1.1336 1.6560	**0.9914** 1.0397 1.2268
1000	**0.4709** 6.5971 8.8302	**0.4743** 4.8488 6.2497	**0.5690** 3.5609 4.5436	**0.6681** 2.5209 3.4672	**0.7810** 1.5452 2.4592	**0.9246** 1.1450 1.6925	**0.9915** 1.0424 1.2420

Table 1. W prompt non-redeposition fractions (top numbers in each cell) for the case with multiple ionizations but without the electric field. The middle number in each cell gives average ion charge of promptly redeposited W ions when they hit the surface, the bottom number – average ion charge of W non-redeposited ions at the first local minimum of the orbit (in the y-direction). B-field is parallel to the surface.

p→ Te (eV)↓	0.01	0.03	0.1	0.3	1	3	10
3	**0** 1.1346 NaN	**3.0E-5** 1.1373 2.2748	**0.0092** 1.1425 2.0207	**0.0532** 1.1008 1.8531	**0.2212** 1.0386 1.2629	**0.5287** 1.0134 1.0653	**0.8023** 1.0036 1.0170
10	**0** 1.5230 NaN	**3.2E-5** 1.5095 3.7673	**0.0118** 1.5169 3.0351	**0.1154** 1.4310 2.3491	**0.3145** 1.2156 1.8496	**0.5609** 1.0792 1.3393	**0.8073** 1.0250 1.0990
30	**0** 1.8452 NaN	**5.0E-5** 1.8202 5.0335	**0.0191** 1.8220 3.9139	**0.1431** 1.6662 3.0437	**0.3674** 1.3640 2.2031	**0.5853** 1.1407 1.5593	**0.8124** 1.0551 1.2206
100	**0** 2.0221 NaN	**1.0E-4** 1.9931 5.5296	**0.0220** 1.9855 4.3484	**0.1583** 1.7949 3.3726	**0.3921** 1.4437 2.3902	**0.5983** 1.1770 1.6713	**0.8140** 1.0551 1.2206
300	**0** 2.0950 NaN	**4.5E-5** 2.0630 6.0374	**0.0226** 2.0549 4.5028	**0.1620** 1.8528 3.4826	**0.4011** 1.4811 2.4711	**0.6060** 1.1966 1.7298	**0.8151** 1.0619 1.2433
1000	**0** 2.1366 NaN	**6.8E-5** 2.1008 6.1715	**0.0220** 2.0930 4.5822	**0.1632** 1.8864 3.5167	**0.4074** 1.5079 2.5124	**0.6111** 1.2102 1.7677	**0.8174** 1.0656 1.2623

Table 2. W prompt non-redeposition fractions (top numbers in each cell) for the case with multiple ionizations and electric field from Stangeby's MPS model for $\alpha = 3°$ and $R_E=0.3$. The middle and bottom numbers in each cell give the same quantities as in Table 1. NaN values imply that there were no promptly non-redeposited orbits, as all orbits intersected the target during the first gyration.

p→ Te (eV)↓	0.01	0.03	0.1	0.3	1	3	10
3	**0** 2.9514	**0** 3.8938	**1.4E-4** 5.0500	**0.0108** 5.8856	**0.1326** 6.2094	**0.4457** 6.2814	**0.7620** 6.3170
10	**0** 3.8830	**0** 5.1394	**8.7E-5** 6.7230	**0.0203** 7.9178	**0.1819** 7.6396	**0.4689** 6.9014	**0.7654** 6.5162
30	**0** 4.6486	**0** 6.1722	**4.1E-5** 8.1504	**0.0213** 9.5930	**0.2086** 8.8578	**0.4860** 7.4716	**0.7691** 6.7090
100	**0** 5.0504	**0** 6.7200	**2.5E-5** 8.8910	**0.0207** 10.508	**0.2188** 9.5236	**0.4964** 7.8156	**0.7694** 6.8160
300	**0** 5.2148	**0** 6.9564	**1.0E-5** 9.2116	**0.0201** 10.871	**0.2229** 9.8384	**0.5012** 7.9624	**0.7721** 6.8838
1000	**0** 5.2822	**0** 7.0534	**1.3E-5** 9.347	**0.0198** 11.064	**0.2255** 10.043	**0.5049** 8.1090	**0.7721** 6.9398

Table 3. W total non-redeposition fractions (top numbers in each cell) for the case with multiple ionizations and electric field from Stangeby's MPS model for $\alpha = 3°$ and R_E=0.3. In difference to Tables 1 and 2, only 2 numbers are given in each cell: top numbers give non-redeposition fractions and bottom numbers give energy amplification factors for W circulating in the MPS (see text for details).

p→ Te (eV)↓	0.01	0.03	0.1	0.3	1	3	10
3	**0** 3.9248	**1.2E-4** 4.7960	**0.0128** 6.2072	**0.0545** 6.9276	**0.2163** 7.0498	**0.5290** 7.0544	**0.8036** 7.0560
10	**0** 5.2320	**4.9E-6** 6.2072	**0.0077** 8.1888	**0.1049** 9.1268	**0.3025** 8.3630	**0.5586** 7.5622	**0.8079** 7.2228
30	**0** 6.2818	**0** 7.3910	**0.0060** 9.9332	**0.1131** 10.920	**0.3517** 9.4886	**0.5818** 8.0532	**0.8122** 7.3696
100	**0** 6.8596	**0** 8.0322	**0.0047** 10.828	**0.1161** 11.859	**0.3718** 10.131	**0.5933** 8.3482	**0.8141** 7.4722
300	**0** 7.1002	**0** 8.3028	**0.0043** 11.175	**0.1162** 12.280	**0.3785** 10.415	**0.5984** 8.4974	**0.8150** 7.5272
1000	**0** 7.2316	**0** 8.4530	**0.0038** 11.380	**0.1148** 12.501	**0.3842** 10.619	**0.6045** 8.6090	**0.8166** 7.5566

Table 4. W total non-redeposition fractions (top numbers in each cell) for the case with multiple ionizations and electric field from Brooks' MPS model for $\alpha = 3°$ and R_E=0.3. Numbers in cells give the same quantities as in Table 3.